Modern Physics Letters B
2050233 (19 pages)
© World Scientific Publishing Company
DOI: 10.1142/S0217984920502334

Mod. Phys. Lett. B Downloaded from www.worldscientific.com
by CHALMERS UNIVERSITY OF TECHNOLOGY on 04/18/20. Re-use and distribution is strictly not permitted, except for Open Access articles.

A full-scale computational study on the electrodynamics of a rigid particle in an optically induced dielectrophoresis chip

Liuyong Shi, Xiaoming Shi and Teng Zhou*

Mechanical and Electrical Engineering College,
Hainan University, Haikou 570228, Hainan, China
**zhouteng@hainanu.edu.cn*

Zhenyu Liu

Changchun Institute of Optics, Fine Mechanics and Physics (CIOMP),
Chinese Academy of Science, Changchun 130033, Jilin, China

Zhiyuan Liu

Key Laboratory of Tropical Biological Resources of Ministry of Education,
Ocean College, Hainan University, Haikou 570228, Hainan, China

Sangwoo Joo†

School of Mechanical Engineering, Yeungnam University,
Gyongsan 712-719, Korea
swjoo@yu.ac.kr

Received 19 December 2019
Revised 1 February 2020
Accepted 5 February 2020
Published 16 April 2020

f A transient continuum model of the ODEP chip containing single circular particle inside is constructed based on multi-physical field coupling. The dielectrophoresis force and liquid viscous resistance acting on particle are calculated by employing the full Maxwell stress tensor. The coupled flow field, electric field and particle are solved by the arbitrary Lagrange–Euler (ALE) method simultaneously. The throughout dynamic process of particle in the ODEP chip is demonstrated, and the effect of several critical parameters on particle electrodynamics is illuminated. The additional disturbing effect of the photoconductive layer on the electric field as well as the micro-channel wall on the flow field is presented to clarify the particle motion in the vertical direction. The results in this study provide a detailed understanding of the particle dynamics in the ODEP chip.

Keywords: Microfluidics; electrodynamics; optically induced dielectrophoresis (ODEP); Maxwell stress tensor (MST).

*,†Corresponding authors.

Mod. Phys. Lett. B Downloaded from www.worldscientific.com
by CHALMERS UNIVERSITY OF TECHNOLOGY on 04/18/20. Re-use and distribution is strictly not permitted, except for Open Access articles.

1. Introduction

Efficient manipulation of small particles has been the core technology in micro-nano scientific research and manufacturing. With the rapid development in biomedical areas, much attention has been focused on the detection and tracking as well as further manipulation of biological particles.[1–5] The dielectrophoresis, action of particles due to a spatially inhomogeneous electric field,[6–9] is often utilized to manipulate charged and neutral particles, including cells, viruses, DNAs, and proteins. In addition to its merits of non-contact and low damage as optical tweezer or magnetic tweezer, the dielectrophoresis technology can also meet the requirements of massive and high-efficiency manipulation for biological particles, thus it has achieved considerable developments.[10–14]

Generally, a traditional dielectrophoresis chip is designed for some specific application needs, such as particle capture, separation or transport and requires pre-implantation of fixed microelectrodes inside the chip. If the complicated manipulation of particles is needed, microelectrodes with an elaborate structure construction are often designed, which inevitably generates increased complexity of chip processing and manufacturing. At the same time, after the production process is completed, its operating function is uniquely determined, which also reduces its flexibility. To solve these problems, Chiou *et al.* proposed the optically-induced dielectrophoresis (ODEP) in 2005, also known as Optoelectronic Tweezer (OET).[15–18] The structure of ODEP chip resembles a sandwich; the micro-channel and the photoconductive layer are sandwiched between the top and bottom indium tin oxide (ITO) glass (glass matrix with ITO film). The photoconductive material layer is made from hydrogenated amorphous silicon a-Si:H. Alternating current (AC) voltage is applied to both ITO films on the chip. When there is no light source to irradiate the photoconductive material layer, the middle area of the chip is governed by a uniform electric field, at which moment the chip is actually equivalent to a parallel plate capacitor, with most of the voltage drop on the photoconductive layer. When a light source is irradiated on the photoconductive material layer, the material conductivity in the illumination area increases sharply, resulting in different voltage drops on the light and the dark areas. A non-uniform electric field is thus generated inside the chip, which is the essential condition for dielectrophoretic manipulation of particles. Benefited from the continuous improvement of the digital micro-mirror device (DMD), optical pattern illuminated on the photoconductive material can be accurately depicted, so that various forms of virtual electrodes can be easily designed, greatly improving the flexibility of chip design and reducing its processing cost.[19–22]

The ODEP has been studied further by a number of numerical simulations and experimental observations.[23–34] In numerical studies, the point dipole method (PDM) used to be employed to calculate the dielectrophoresis force acting on a particle. This method approximates a particle as a point mass, without considering its volume and coupling effect with the flow and electric fields. Discrepancies thus

Mod. Phys. Lett. B Downloaded from www.worldscientific.com
by CHALMERS UNIVERSITY OF TECHNOLOGY on 04/18/20. Re-use and distribution is strictly not permitted, except for Open Access articles.

result between the dynamic calculations and the actual motion of particles, which would impair the precise control of particle motion and the design of microchip structure. Most experimental reports on the other hand focus on the final performance of particle manipulations, seldom shows the entire particle motion, which is essential for understanding the dynamical mechanism of particles in ODEP chip.

In this study, a transient arbitrary Lagrange–Euler (ALE) finite-element computation of a circular rigid particle in an ODEP chip is performed for a fully coupled nonlinear system. The dielectrophorestic force and liquid resistance acting on particle are calculated for the first time by the full Maxwell stress tensor (MST) method in the ODEP model, though it has been employed in the traditional dielectrophoresis numerical model.[35–37] By integrating the stress tensor on the entire particle surface, this method predicts forces exerting on particle with various shapes and sizes more precisely than PDM. The dynamics in the particle evolution is detailed, providing further insight into the ODEP and a basis for improving particle manipulation.

2. Numerical Model

2.1. *Model geometry and parameters*

Based on the sandwich structure of an ODEP chip described above, we construct a two-dimensional ODEP chip model containing a rigid circular particle, as shown in Fig. 1. The solid lines AB and CD on the top and bottom edges represent ITO

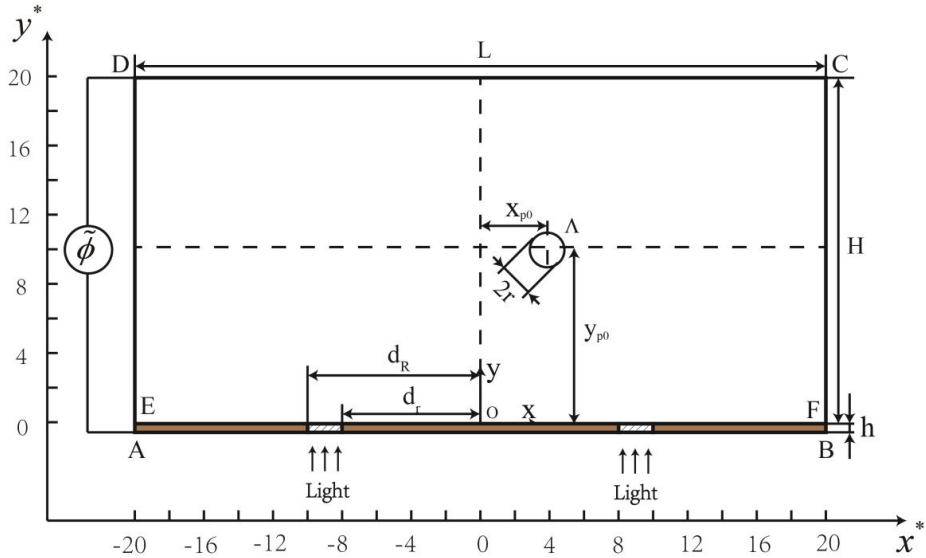

Fig. 1. The two-dimensional schematic diagram of the ODEP chip containing single circular particle. The left and bottom coordinate X^*OY^* in this figure is dimensionless result of the original coordinate system XOY by using characteristic length.

Mod. Phys. Lett. B Downloaded from www.worldscientific.com
by CHALMERS UNIVERSITY OF TECHNOLOGY on 04/18/20. Re-use and distribution is strictly not permitted, except for Open Access articles.

thin film electrodes, where an AC voltage is applied. The region CDEF represents microfluidic channel with the height $H = 100\ \mu$m, the length $L = 200\ \mu$m. The thin layer ABFE channel bottom represents the photoconductive layer with the thickness $h = 2\ \mu$m. The intrinsic hydrogenated amorphous silicon α-Si:H is selected as the photoconductive layer material as usual. The microfluidic channel is filled with the deionized aqueous solution of its density $\rho_f = 1000\ \mathrm{kg/m^3}$, the absolute permittivity $\varepsilon_f = 7.08 \times 10^{-10}$ F/m, the conductivity $\sigma_f = 1 \times 10^{-3}$ S/m and the dynamic viscosity $\eta = 1 \times 10^{-3}$ Pa $\cdot$ s. A polystyrene (PS) microsphere is selected as the object particle, with its density, shear modulus, bulk modulus, absolute permittivity and conductivity as $\rho_p = 1050\ \mathrm{kg/m^3}$, $G_P = 1 \times 10^9$ Pa, $B_P = 1 \times 10^4$ Pa, $\varepsilon_p = 2.3 \times 10^{-11}$ F/m, $\sigma_p = 4 \times 10^{-4}$ S/m, respectively. The particle radius is varied as $r_P = 5$, 7.5, 10 μm, or in the dimensionless form as $r_P^* = 1$, 1.5, 2 in this study, and the starting position of particle center is located at (X_{p0}, Y_{p0}). The microfluidic channel sizes are also dimensionless as $L^* = 40$, $H^* = 20$, respectively.

The two-dimensional Cartesian coordinate system XOY is established at the center of EF, on the bottom of the microfluidic channel. At the same time, in order to generalize its electrodynamics process of particle, we have also established a dimensionless coordinate system X^*OY^* via characteristic length, whose origin of coordinates coincides with XOY, as shown in Fig. 1. The ring-shaped light source is used to illuminate the photoconductive material from bottom-up direction. The two-dimensional distribution of the illumination areas is shown as the light areas in Fig. 1, and the remaining areas except for the bright areas in the photoconductive layer are considered as the dark areas. The center point of the ring-shaped light source is sitting on the Y-axis of the coordinate system, and its inner and outer diameters are $d_r = 40\ \mu$m, $d_R = 50\ \mu$m, respectively. The absolute permittivity of α-Si:H as the photoconductive material is $\varepsilon = 11.7\varepsilon_0$, ε_0 is the absolute permittivity in vacuum. In other word, the permittivity in both the illumination area and the dark area is considered as equal, whereas their conductivities differ greatly, in the bright region the conductivity is $\sigma_l = 0.21$ S/m, $\sigma_d = 6.7 \times 10^{-5}$ S/m for the dark region.

2.2. *Physical fields and boundary conditions*

AC voltage is applied on the top and bottom boundaries AB, CD in this model, and its alternative frequency is $f = 10^5$ Hz. The electric field distribution can be solved by the Maxwell equations in quasi-static form, considering that the model size is far smaller than the electromagnetic wavelength.

$$\nabla \cdot (\tilde{\varepsilon}_f \nabla \widetilde{\phi}_f) = 0 \quad \text{in } \Omega_f\,, \tag{1}$$

$$\nabla \cdot (\tilde{\varepsilon}_p \nabla \widetilde{\phi}_p) = 0 \quad \text{in } \Omega_p\,, \tag{2}$$

$$\nabla \cdot (\tilde{\varepsilon}_d \nabla \widetilde{\phi}_d) = 0 \quad \text{in } \Omega_d\,, \tag{3}$$

$$\nabla \cdot (\tilde{\varepsilon}_l \nabla \widetilde{\phi}_l) = 0 \quad \text{in } \Omega_l\,. \tag{4}$$

Mod. Phys. Lett. B Downloaded from www.worldscientific.com
by CHALMERS UNIVERSITY OF TECHNOLOGY on 04/18/20. Re-use and distribution is strictly not permitted, except for Open Access articles.

Among them, the complex permittivities of fluid, particle, bright area and dark area are, respectively, $\tilde{\varepsilon}_f = \varepsilon_f - j\sigma_f/\omega$, $\tilde{\varepsilon}_p = \varepsilon_p - j\sigma_p/\omega$, $\tilde{\varepsilon}_l = \varepsilon - j\sigma_l/\omega$, $\tilde{\varepsilon}_d = \varepsilon - j\sigma_d/\omega$, the complex potentials in fluid, particle, bright area and dark area are $\widetilde{\phi}_f$, $\widetilde{\phi}_p$, $\widetilde{\phi}_l, \widetilde{\phi}_d$, respectively. The superscript "$\sim$" represents a complex variable. The angular frequency of AC is $\omega = 2\pi f$, $j = \sqrt{-1}$, imaginary part unit; $\Omega_f, \Omega_p, \Omega_l, \Omega_d$ represent the fluid domain, particle domain, optical bright domain and optical dark domain, respectively.

The boundary conditions for the electric field:

$$\tilde{\phi} = \phi_0,\ \phi_0 = 10, 30, 50 \text{ V on AB and } \tilde{\phi} = 0 \quad \text{on CD}, \tag{5}$$

$$\mathbf{n} \cdot \widetilde{\varepsilon}_f \nabla \widetilde{\phi}_f = 0 \quad \text{on AD, BC}, \tag{6}$$

$\mathbf{n}$ represents the unit normal vector.

To ensure the continuity of electric field in the interface between particle and fluid,

$$\widetilde{\phi}_f = \widetilde{\phi}_p \text{ on } \Lambda, \quad \Lambda \text{ is the particle boundary}, \tag{7}$$

$$\mathbf{n} \cdot \nabla \widetilde{\phi}_f = \frac{\widetilde{\varepsilon}_p}{\widetilde{\varepsilon}_f} \mathbf{n} \cdot \nabla \widetilde{\phi}_p \text{ on } \Lambda\,. \tag{8}$$

We use the continuity equation and the Stokes equation to describe fluid flow. Considering the small Reynolds number of fluid flow in this study, the inertia term can be neglected. In the process of calculation, we set DE and CF as open boundaries, CD and EF as wall boundaries.

$$\nabla \cdot \mathbf{u} = 0 \quad \text{in } \Omega_f\,, \tag{9}$$

$$\rho_f \frac{\partial \mathbf{u}}{\partial t} = -\nabla \mathrm{p} + \eta \nabla^2 \mathbf{u} \quad \text{in } \Omega_f\,. \tag{10}$$

$\mathbf{u}$ is fluid velocity and p is fluid pressure, t is time variable.

In this model, the PS particle is defined as a circular rigid model. Because the density of PS is close to that of deionized aqueous solution, the gravity and buoyancy on particle can be regarded as offset each other. In addition, considering the particle size employed here is in the order of micron, the Brownian force on particle can also be neglected. Therefore, we just need to take into account the time-averaged dielectrophoresis force and liquid viscous resistance acting on particle. These two forces can be obtained by integrating Maxwell stress tensor $\mathbf{T}_M$ and hydrodynamic stress tensor $\mathbf{T}_H$ throughout the particle surface. The time-averaged dielectrophoresis force $\mathbf{F}_{\mathrm{DEP}}$ and liquid viscous resistance $\mathbf{F}_H$ on particle are expressed as follows:

$$\mathbf{F}_{\mathrm{DEP}} = \int \mathbf{T}_{\mathbf{M}} \cdot \mathbf{n} dS = \int \frac{\varepsilon_f}{4} [(\widetilde{\mathbf{E}}\widetilde{\mathbf{E}}' + \widetilde{\mathbf{E}}'\widetilde{\mathbf{E}}) - \left|\widetilde{\mathbf{E}}\right|^2 \mathbf{I}] \cdot \mathbf{n} dS \tag{11}$$

$$\mathbf{F}_H = \int \mathbf{T}_H \cdot \mathbf{n} dS = \int [-p\mathbf{I} + \eta(\nabla \mathbf{u} + (\nabla \mathbf{u})^T)] \cdot \mathbf{n} dS\,. \tag{12}$$

Mod. Phys. Lett. B Downloaded from www.worldscientific.com
by CHALMERS UNIVERSITY OF TECHNOLOGY on 04/18/20. Re-use and distribution is strictly not permitted, except for Open Access articles.

$\widetilde{\mathbf{E}}$ is the intensity of the electric field, $\widetilde{\mathbf{E}}'$ is the complex conjugate of $\widetilde{\mathbf{E}}$.

$$\widetilde{\mathbf{E}} = -\nabla\widetilde{\phi}\,. \tag{13}$$

Considering that a circular particle is employed here, so its rotation motion is laid aside. The translation motion and position change of particle can be described by the following equation:

$$m_p \frac{d\mathbf{U}_p}{dt} = \mathbf{F}_H + \mathbf{F}_{\mathrm{DEP}}\,, \tag{14}$$

$$x_p = x_{p0} + \int_0^t \mathbf{U}_p dt\,. \tag{15}$$

m_p represents the particle mass, x_p represents the x-coordinate position of particle center, x_{p0} means its starting position of particle center and $\mathbf{U}_p$ represents the translation velocity of particle.

2.3. *Dimensionless method*

The particle radius $r_p = 5\ \mu$m as the characteristic length, $U_\infty = (\varepsilon_f \phi_\infty^2)/(\eta a)$ as the characteristic velocity and $\phi_\infty = R_0 T/F$ as the characteristic potential are introduced to normalize the aforementioned governing equations. Firstly, some basic physical quantities are dealt as follows:

$$\mathbf{x} = a\mathbf{x}^*, \quad \mathbf{u} = U\infty\mathbf{u}^*, \quad p = \eta U_\infty p^*/a, \quad \widetilde{\phi} = \phi_\infty \widetilde{\phi}^*\,,$$
$$t = at^*/U_\infty, \quad \mathrm{Re}\ = \rho_f a U_\infty/\eta\,.$$

Here, R_0 is the universal gas constant, T is the absolute temperature, F is the Faraday constant and Re is the Reynolds number, respectively. The superscript "$*$" denotes a dimensionless variable.

Correspondingly, all the governing equations can be described in detail as follows:

$$\nabla^* \cdot (\tilde{\varepsilon}_f^* \nabla^* \widetilde{\phi}_f^*) = 0 \quad \text{in } \Omega_f\,, \tag{16}$$

$$\nabla^* \cdot (\tilde{\varepsilon}_p^* \nabla^* \widetilde{\phi}_p^*) = 0 \quad \text{in } \Omega_p\,, \tag{17}$$

$$\nabla^* \cdot (\tilde{\varepsilon}_d^* \nabla^* \widetilde{\phi}_d^*) = 0 \quad \text{in } \Omega_d\,, \tag{18}$$

$$\nabla^* \cdot (\tilde{\varepsilon}_l^* \nabla^* \widetilde{\phi}_l^*) = 0 \quad \text{in } \Omega_l\,, \tag{19}$$

$$\widetilde{\phi}_f^* = \phi_0/\phi_\infty \quad \text{on AB and } \widetilde{\phi}_f^* = 0 \quad \text{on CD}\,, \tag{20}$$

$$\mathbf{n} \cdot \widetilde{\varepsilon}_f^* \nabla^* \widetilde{\phi}_f^* = 0 \quad \text{on AD and BC}\,, \tag{21}$$

$$\widetilde{\phi}_f^* = \widetilde{\phi}_p^* \quad \text{on } \Lambda\,, \tag{22}$$

Mod. Phys. Lett. B Downloaded from www.worldscientific.com
by CHALMERS UNIVERSITY OF TECHNOLOGY on 04/18/20. Re-use and distribution is strictly not permitted, except for Open Access articles.

$$\mathbf{n}\cdot\nabla^*\widetilde{\phi}_f^* = \frac{\widetilde{\varepsilon}_p^*}{\widetilde{\varepsilon}_f^*}\mathbf{n}\cdot\nabla^*\widetilde{\phi}_p^* \quad \text{on } \Lambda\,, \tag{23}$$

$$\nabla^*\cdot\mathbf{u}^* = 0 \quad \text{in } \Omega_f\,, \tag{24}$$

$$\mathrm{Re}\frac{\partial\mathbf{u}^*}{\partial t^*} = -\nabla^* p^* + \eta\nabla^{*2}\mathbf{u}^* \quad \text{in } \Omega_f\,, \tag{25}$$

$$\widetilde{\varepsilon}_f^* = 1 - j\sigma_f/(\omega\varepsilon_f), \quad \widetilde{\varepsilon}_p^* = 1 - j\sigma_p/(\omega\varepsilon_p),$$

$$\widetilde{\varepsilon}_d^* = 1 - j\sigma_d/(\omega\varepsilon), \quad \widetilde{\varepsilon}_l^* = 1 - j\sigma_l/(\omega\varepsilon)\,,$$

$$\mathbf{F}_{\mathrm{DEP}}^* = \int \mathbf{T}_{\mathbf{M}}^*\cdot\mathbf{n}dS^* = \int \frac{1}{4}[(\widetilde{\mathbf{E}}^*\widetilde{\mathbf{E}}'^* + \widetilde{\mathbf{E}}'^*\widetilde{\mathbf{E}}^*) - |\widetilde{\mathbf{E}}^*|^2\mathbf{I}]\cdot\mathbf{n}dS^*\,, \tag{26}$$

$$\mathbf{F}_H^* = \int \mathbf{T}_{\mathbf{H}}^*\cdot\mathbf{n}dS^* = \int [-p^*\mathbf{I} + (\nabla^*\mathbf{u}^* + (\nabla^*\mathbf{u}^*)^T)]\cdot\mathbf{n}dS^*\,, \tag{27}$$

$$m_p^*\frac{d\mathbf{U}_p^*}{dt^*} = \mathbf{F}_H^* + \mathbf{F}_{\mathrm{DEP}}^*\,, \tag{28}$$

$$x_P^* = x_{P0}^* + \int_0^{t^*}\mathbf{U}_P^* dt^* \tag{29}$$

$$\mathbf{F}_H = \eta U_\infty\mathbf{F}_H^*, \quad \mathbf{T}_H = \eta U_\infty\mathbf{T}_H^*/a, \quad m_p = \eta a m_p^*/U_\infty\,.$$

Eventually, a commercial finite-element package COMSOL (version 5.3) operating in a high performance cluster is employed to solve the above-mentioned governing equations by using the ALE method. The initial values of the fluid velocity, pressure, particle velocity in relative computational domains are set to zero. The starting position of particle center is placed at ($x_{p0}^* = 4, y_{p0}^* = 10$). To verify the reliability of above model, we calculate the spatial distribution of the electric field

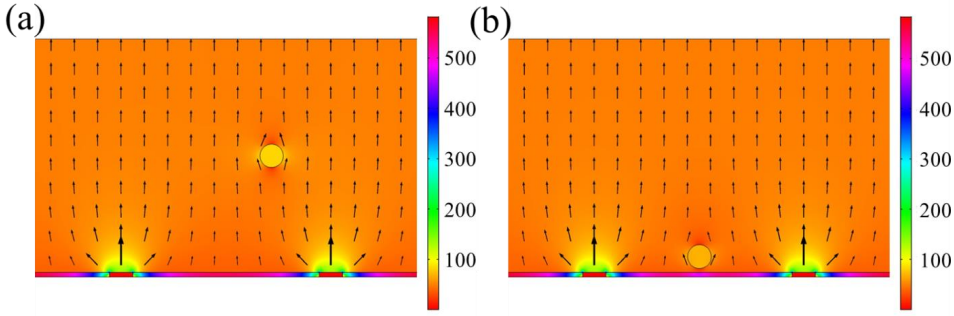

Fig. 2. (Color online) The spatial distribution of electric field intensity inside the ODEP chip at the different times of particle motion (a) $t = 0$ s, (b) $t = 1.362$ s. The circle in the figure represents the particle, the black arrows indicate the direction of electric field, and the color scales on the right side of the figure denote the electric field intensity, and it has been dimensionless. External AC voltage $\tilde{\phi} = 30$ V, the dimensionless particle radius $r_P^* = 1$.

Mod. Phys. Lett. B Downloaded from www.worldscientific.com
by CHALMERS UNIVERSITY OF TECHNOLOGY on 04/18/20. Re-use and distribution is strictly not permitted, except for Open Access articles.

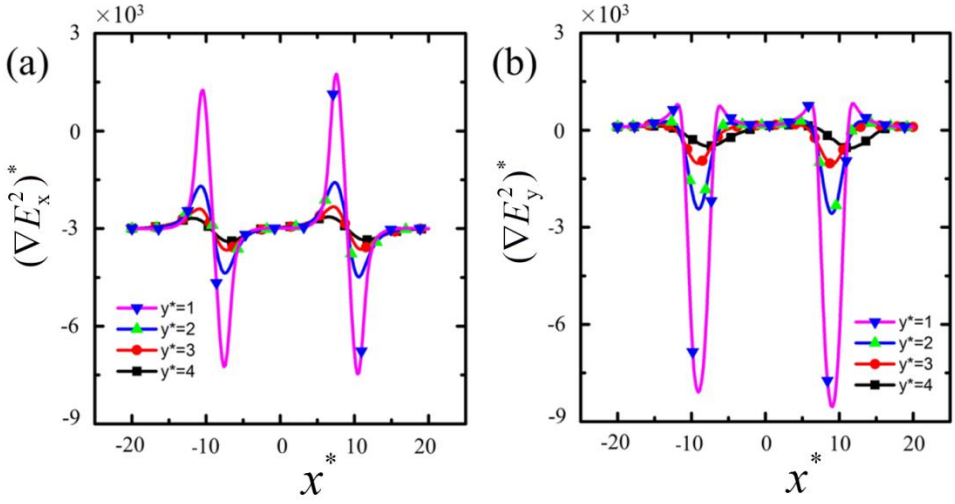

Fig. 3. (Color online) X-direction distribution of electric field square gradient at different height from EF, the bottom edge of micro-channel. (a) The X-component of electric field square gradient (∇E_x^2). (b) The Y-component of electric field square gradient (∇E_y^2). y^* denotes the height from EF edge, which has been dimensionless. Applied AC voltage $\tilde{\phi} = 30$ V, the dimensionless particle radius $r_P^* = 1$. At this point, the particle is fixed in its starting position.

intensity inside the ODEP chip and the X-direction distribution of the electric field square gradient, as shown in Figs. 2 and 3, respectively, and the electric field distribution in these two figures is highly consistent with the results of Refs. 38 and 39, which proves that our model is trustworthy. Based on this, we proceed to Sec. 3.

3. Results and Discussion

Based on the above model and parameters, we use ALE method to simultaneously solve the coupled flow field, electric field and the particle module, and explicate the influence of particle size and applied voltage on the electrodynamics of particle, such as the dielectrophoresis force, particle trajectory, particle velocity, acceleration and so on.

3.1. *Dielectrophoresis force*

Figure 4 shows the dielectrophoresis force acting on particle with different radius depending on particle center position under the same applied voltage. As can be seen from Fig. 4(a), the X-component $F^*_{\mathrm{DEP}x}$ of dielectrophoresis force maintains as the negative value during the whole movement process, which indicates that the dielectrophoresis force component in the X-direction keeps left-oriented; and its magnitude of $F^*_{\mathrm{DEP}x}$ is relatively large at the initial moment (here, the magnitude only means its numerical size, not including its direction, all the same below). As the particle moves closer to the center point of the optical ring, the

Mod. Phys. Lett. B Downloaded from www.worldscientific.com
by CHALMERS UNIVERSITY OF TECHNOLOGY on 04/18/20. Re-use and distribution is strictly not permitted, except for Open Access articles.

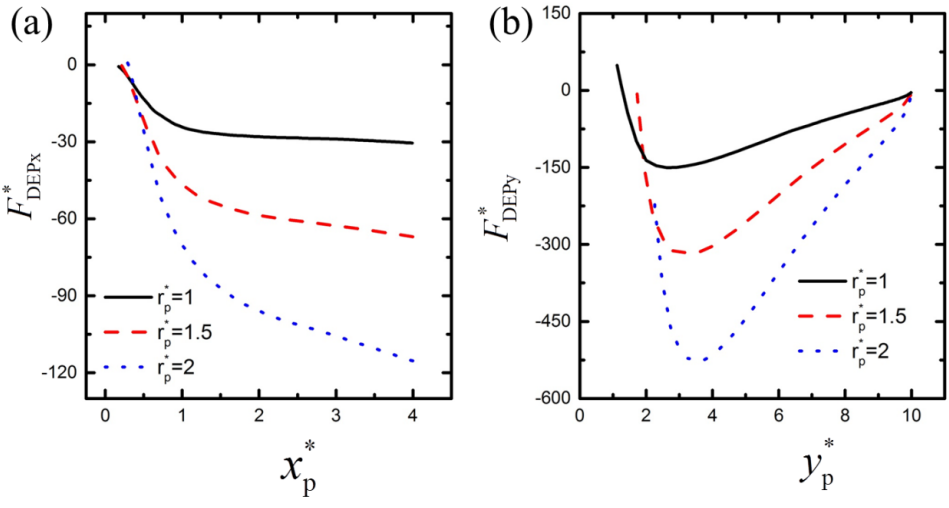

Fig. 4. (Color online) The dielectrophoresis force acting on particle with radius $r^*_P = 1$, 1.5, 2 depending on particle center position. (a) The X-component $F^*_{\mathrm{DEP}x}$ of the dielectrophoresis force depending on the particle center position x^*_p. (b) The Y-component $F^*_{\mathrm{DEP}y}$ of the dielectrophoresis force depending on particle center position y^*_p. The starting position of particle center locates on ($x^*_{p0} = 4$, $y^*_{p0} = 10$) and the applied AC voltage $\tilde{\phi} = 30$ V.

dielectrophoresis force decreases rapidly, and finally drops to zero. As can be seen from Fig. 4(b), except for a small distance near the bottom edge of the microchannel (nearly $y^*_P = 1$, where the particle itself has a certain diameter), the Y-component of dielectrophoresis force $F^*_{\mathrm{DEP}y}$ also maintains as the negative value during most of particle movement, which indicates that the dielectrophoresis force component keeps downward basically; And its magnitude is close to zero at the first moment, then increases rapidly with the particle moving downward, reaches its maximum value near the bottom $y^* = 3$ approximately (namely 15 microns away from the bottom edge EF); and when the particle is very close to the bottom, the dielectrophoresis force component turns to decrease rapidly, even may become a positive value, in other word, its direction turns upward. In addition, with the larger particle radius, generally, its magnitude of dielectrophoresis force component increases markedly, but those variation curves of dielectrophoresis force for particles with different radius exhibit similar trends basically.

Figure 5 shows the dielectrophoresis force acting on particle with the same radius depending on the particle center position at the different applied voltages. It can be seen from the figure that the magnitude of dielectrophoresis forces including $F^*_{\mathrm{DEP}x}, F^*_{\mathrm{DEP}y}$ are almost close to zero when the applied voltage is very low, $\tilde{\phi} = 10$ V. With the higher applied voltage, both the dielectrophoresis forces increase significantly, but their change trends are still basically similar with those in Fig. 4. When the applied voltage is adjusted to relatively high, $\tilde{\phi} = 50$ V, the dielectrophoresis force component in Y-direction even change rapidly to a

Mod. Phys. Lett. B Downloaded from www.worldscientific.com
by CHALMERS UNIVERSITY OF TECHNOLOGY on 04/18/20. Re-use and distribution is strictly not permitted, except for Open Access articles.

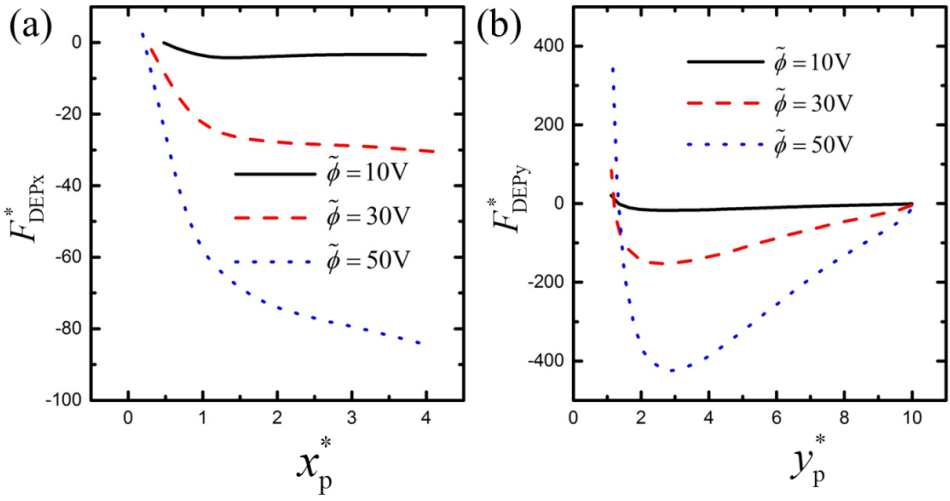

Fig. 5. (Color online) The dielectrophoresis force acting on particle depending on particle center position with applied AC voltages $\tilde{\phi}$ = 10 V, 30 V, 50 V. (a) The X-component $F^*_{\mathrm{DEP}x}$ of the dielectrophoresis force depending on the particle center position x^*_p. (b) The Y-component $F^*_{\mathrm{DEP}y}$ of the dielectrophoresis force depending on the particle center position y^*_p. The starting position of the particle center locates on ($x^*_{p0} = 4$, $y^*_{p0} = 10$) and the dimensionless particle radius $r^*_P = 1$.

positive value when particle approaches the bottom edge EF, which means that the dielectrophoresis force component turns upward and becomes a hindering factor for the downward movement of particle.

According to the classical point dipole method (PDM), the dielectrophoresis force acting on a particle can be calculated by Eq. (30). According to Eq. (30), the changing trends of the dielectrophoresis force mentioned above can be explained qualitatively and conveniently.

$$\mathbf{F}_{\mathrm{DEP}} = 2\pi\varepsilon_f r_p^3 \,\mathrm{Re}(\widetilde{f}_{\mathrm{CM}})\nabla \left|\widetilde{\mathbf{E}}_{\mathrm{rms}}\right|^2 \tag{30}$$

$$\widetilde{f}_{\mathrm{CM}} = \frac{\tilde{\varepsilon}_p - \tilde{\varepsilon}_f}{\tilde{\varepsilon}_p + 2\tilde{\varepsilon}_f} \tag{31}$$

Here, $\widetilde{f}_{\mathrm{CM}}$ represents the complex Clausius–Mossotti factor, a parameter describing the polarization degree of particle and solution. $\mathrm{Re}(\widetilde{f}_{\mathrm{CM}})$ represents the real part of $\widetilde{f}_{\mathrm{CM}}$. If it is a positive real number, that means the polarization degree of particle exceeds that of solution, the particle will move toward the strong electric field region by the action of positive dielectric electrophoresis force, so-called positive DEP phenomenon. Conversely, when it is a negative real number, the particle will move toward the weak electric field region by the action of negative dielectric electrophoresis force, namely negative DEP phenomenon. $|\widetilde{\mathbf{E}}_{\mathrm{rms}}|$ represents the root mean square of the electric field.

According to those parameters determined in this study, we can calculate that the value of $\mathrm{Re}(\widetilde{f}_{\mathrm{CM}})$ is negative here, $\mathrm{Re}(\widetilde{f}_{\mathrm{CM}}) = -0.38$, that means, the

Mod. Phys. Lett. B Downloaded from www.worldscientific.com
by CHALMERS UNIVERSITY OF TECHNOLOGY on 04/18/20. Re-use and distribution is strictly not permitted, except for Open Access articles.

polarization degree of particle is less than that of solution, so the particle will be dominated by negative dielectrophoresis force and will move toward the weak electric field region. As can be seen from the electric field distribution in Fig. 2, the region near the optical ring demonstrates the strong electric field region, while the outer and inner sides around the optical ring (i.e. the center area of the optical ring) exhibit as the weak electric field region. In addition, since the starting position of particle is adjacent to the right illumination area in the two-dimensional model, the repulsion force in the x-direction from the right illumination area is much greater than that of the left illumination area, so the dielectrophoresis force component $F^*_{\mathrm{DEP}x}$ is larger in magnitude and left-oriented at the starting stage; and when the particle moves to the center area of the optical ring, the repulsive force on particle from both the light areas is almost equal, so the dielectrophoresis force component in the X-direction $F^*_{\mathrm{DEP}x}$ drops rapidly to zero.

It can be seen from Fig. 3 that the gradient of the electric field square is relatively weak for the areas far from the bottom edge EF, and it will become stronger as the position is closer to the bottom of the micro-channel. Therefore, during the downward movement process of particle, when its starting position is far from the bottom, the dielectrophoresis force acting on particle is almost zero in the Y-direction. As the particle gets closer to the bottom, the dielectrophoresis force will increase dramatically with the greater gradient of electric field square. However, when the particle moves down to the bottom, the electric field near the particle will be disturbed by the photoconductive material layer, thus the particle may be subjected to the electrostatic repulsive force from photoconductive material layer, which greatly reduces the total dielectrophoresis force acting on particle, even change its direction from downward to upward. This is not indicated in Fig. 3 because the particle is fixed in its starting position and always far from the photoconductive material layer.

It can also be seen from Eq. (30) that the dielectrophoresis force on particle is proportional to the particle volume, and it will increase obviously with the larger particle radius. The root mean square of the electric field $|\widetilde{\mathbf{E}}_{\mathrm{rms}}|$ also increases obviously under the higher applied voltage for the fixed size of the chip, accordingly, the gradient of the electric field square fluctuates more vigorously, so the dielectrophoresis force also increased significantly according to Eq. (30). In a word, the results of numerical simulation for the dielectrophoresis force exhibit qualitative consistent with the analytical results of the classical PDM.

3.2. *The trajectory of particle center*

Figure 6 shows the effect of particle radius and applied AC voltage on the trajectory of particle center. From the two figures in Fig. 6, it can be seen that when particles depart from the same starting position $(4, 10)$, they will move to the lower left area under the action of dielectrophoresis force, and thus keep close to the center of the optical ring. With the uniform particle radius, as the applied AC voltage rises, the

Mod. Phys. Lett. B Downloaded from www.worldscientific.com
by CHALMERS UNIVERSITY OF TECHNOLOGY on 04/18/20. Re-use and distribution is strictly not permitted, except for Open Access articles.

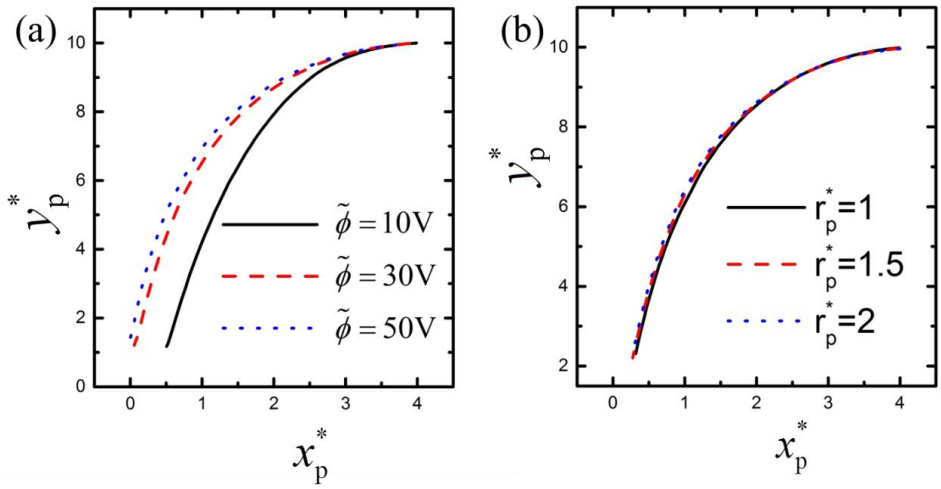

Fig. 6. (Color online) The trajectory of particle center in the case of (a) same radius $r_p^* = 1$, different applied voltage $\tilde{\phi} = 10$ V, 30 V, 50 V, (b) uniform applied voltage $\tilde{\phi} = 30$ V, varied radius $r_p^* = 1, 1.5, 2$. The starting position of particle center locates on ($x_{p0}^* = 4$, $y_{p0}^* = 10$).

final positions of particles will gradually approach the central point of the optical ring ($x_P^* = 0$), as shown in Fig. 6(a). When the applied voltage is fixed, changing the particle radius has little effect on the trajectory of particle center. As shown in Fig. 6(b), the trajectories for particles with three radii basically coincide. We also investigate their trajectories of particles departing from different starting positions, as shown in Fig. 7. It can be seen that, as long as the starting positions of particles are in the surroundings of the optical ring ($-8 \leq x_p^* \leq +8$), the particles will eventually converge near the central point of the optical ring. With the increasing horizontal distance from the center of the optical ring and the height from the bottom edge, the end-position of particles will be closer to the central point of the optical ring. This simulated results of particle trajectory are in agreement with the experimental results in Refs. 28 and 29.

According to the dielectrophoresis force presented above, the particle employed here is subjected to the negative dielectrophoresis force in most of its movement process, so the particle will be repulsed to the weak electric field region. Since the starting position of particle has been already surrounded by the optical ring, it is too difficult to move beyond the optical ring to the outside for particle, but only move toward the central region of the ring. As mentioned in the above section, the dielectrophoresis force of particle is also proportional to the particle volume and the gradient of the electric field square, therefore, those particles with larger radii or immersed in stronger electric field are inclined to be closer to the center point of the optical ring under the action of greater dielectrophoresis force. Different horizontal positions only have little influence on the trajectory during the initial stage of particle motion, after that, the forces acting on particle are almost uniformly, so

Mod. Phys. Lett. B Downloaded from www.worldscientific.com
by CHALMERS UNIVERSITY OF TECHNOLOGY on 04/18/20. Re-use and distribution is strictly not permitted, except for Open Access articles.

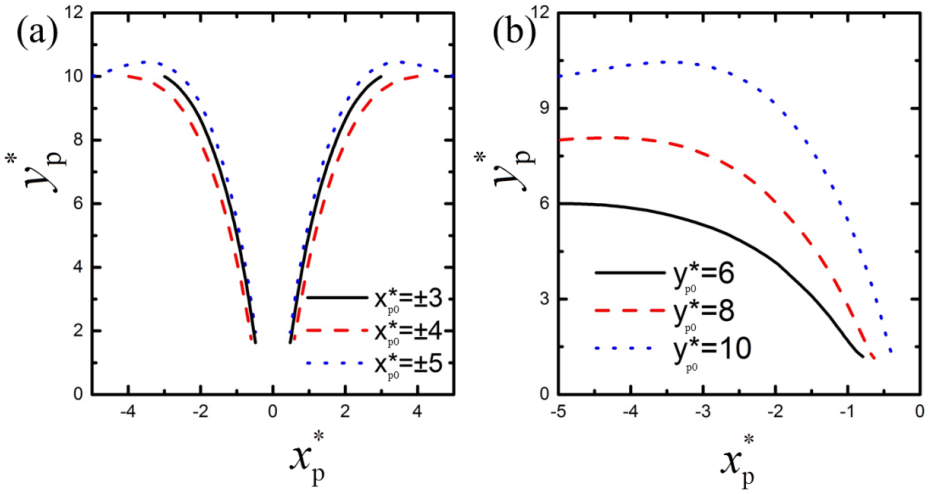

Fig. 7. (Color online) The trajectory of particle center with different starting positions (a) at the same vertical height ($y_{p0}^* = 10$), different horizontal positions ($x_{p0}^* = \pm 3, x_{p0}^* = \pm 4, x_{p0}^* = \pm 5$), (b) at the same horizontal position ($x_{p0}^* = -5$), different vertical heights ($y_{p0}^* = 6, y_{p0}^* = 8$, $y_{p0}^* = 10$). The applied AC voltage $\widetilde{\phi} = 30$ V, the particle radius $r_p^* = 1$.

their trajectories after that are also coincident. When particles depart from different vertical altitudes, those particles with higher starting position will have a longer horizontal motion distance, and their final position will be closer to the center point of the optical ring, but it will take their more time to move. In short, no matter how the starting positions of particles change, as long as they are surrounded by the optical ring at the initial moment, particles will eventually converge to the central region of the optical ring under the action of the negative dielectrophoresis force, which is of positive significance for particle classification and convergence manipulation.

3.3. *The velocity and acceleration of particle translation*

Figure 8 depicts the translation velocity curves of particles with different radii depending on the particle center position. It can be seen from the figure that both the velocity components u_x^*, u_y^* of particles maintain as negative value, that means that the actual velocity direction of particle keeps always opposite to that of the coordinate axis, which is consistent with the simulation results of the dielectrophoresis force and trajectory above. As shown in Fig. 8(a), the particle velocity component u_x^* is initially zero, and then increases rapidly as particle moves toward the center point of the optical ring. During the middle stage of particle motion, its velocity increases slowly, while it decreases rapidly when it approaches the center of the optical ring.

From Fig. 8(b), it can be seen that the particle velocity component u_y^* is almost zero at its starting position; as particle moves downward, this velocity

Mod. Phys. Lett. B Downloaded from www.worldscientific.com
by CHALMERS UNIVERSITY OF TECHNOLOGY on 04/18/20. Re-use and distribution is strictly not permitted, except for Open Access articles.

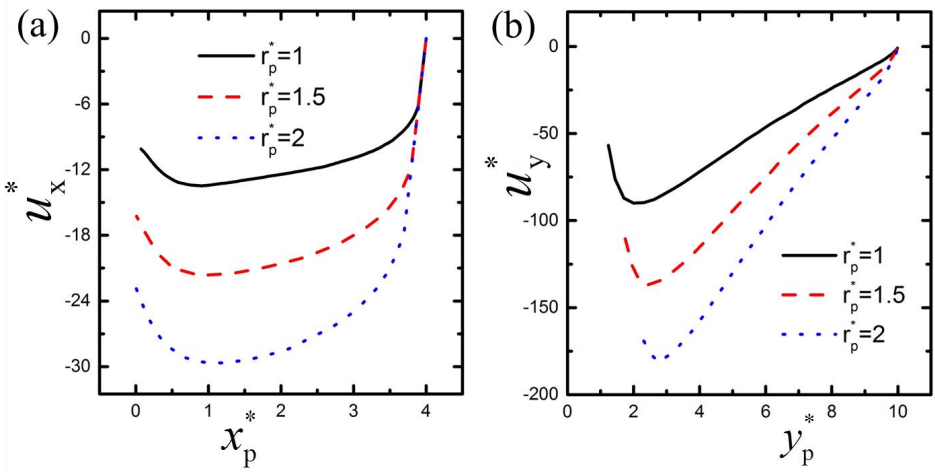

Fig. 8. (Color online) The particle translation velocity with particle radius $r_p^* = 1, 1.5, 2$ depending on particle center position. (a) The X-component u_x^* of the particle velocity depending on particle center position x_P^*. (b) The Y-component $u_y^*$of the particle velocity depending on particle center position y_P^*. The starting position of particle center locates on $(x_{p0}^* = 4, y_{p0}^* = 10)$ and the applied AC voltages $\widetilde{\phi} = 30$ V.

component increases rapidly until it reaches its maximum value near the bottom (i.e., $y^* = 3$, namely 15 microns from the bottom); then, this velocity component decreases rapidly as the particle approaches the bottom edge. With the larger particle radius, the maximum values of velocity components u_x^*, u_y^* increase obviously, but their velocity varying curves of particles with different radius show similar trends basically.

Figure 9 depicts the translation velocity curves of particles depending on the particle center position under adjusting applied AC voltages. It can be seen from this figure that when the applied AC voltage is low $\widetilde{\phi} = 10$ V, both the velocity components is relatively small all the time, which can be attributed to the fact particles are subjected to a feeble dielectrophoresis force; while the applied AC voltage rises to, $\widetilde{\phi} = 30$ V, 50 V, both the velocity components increase obviously, but their changing trends still keep essentially similar with those shown in Fig. 8.

The above-mentioned velocity curves can be explained profoundly by introducing the particle acceleration depending on the particle center position, as shown in Fig. 10. It should be noted that the acceleration in this figure represents the total acceleration of particle translation, which takes into account the acceleration caused by both forces including dielectrophoresis force and liquid viscous resistance, so it can reflect the effect of the resultant force on particle. As shown in Fig. 10(a), during the beginning stage of particle motion, due to the larger dielectrophoresis force and the smaller liquid viscous force (generally the magnitude of liquid viscous resistance is proportional to the particle velocity which is relatively small at this moment), the dielectrophoresis force plays a dominating role, the acceleration

Mod. Phys. Lett. B Downloaded from www.worldscientific.com
by CHALMERS UNIVERSITY OF TECHNOLOGY on 04/18/20. Re-use and distribution is strictly not permitted, except for Open Access articles.

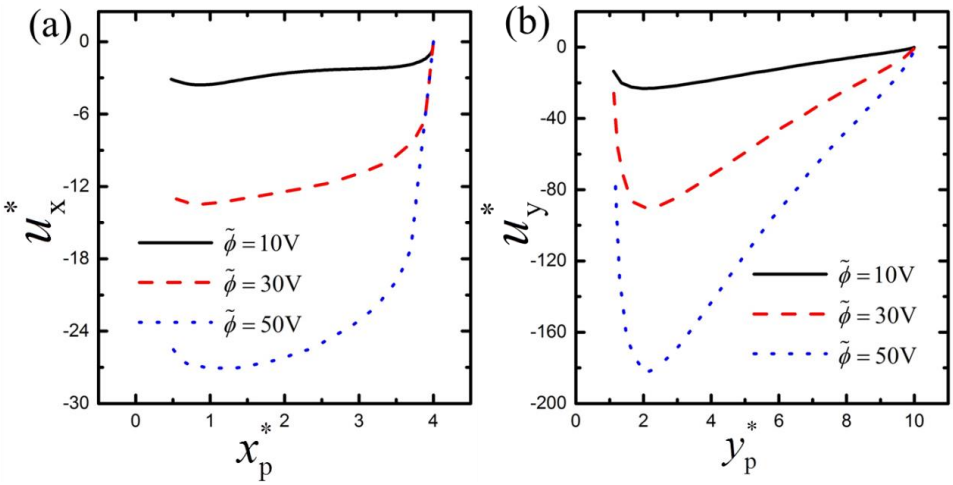

Fig. 9. (Color online) The particle translation velocity at the vary AC voltage $\tilde{\phi} = 10$ V, 30 V, 50 V depending on particle center position. (a) The X-component u_x^* of the particle velocity depending on particle center position x_P^*. (b) The Y-component u_y^* of the particle velocity depending on particle center position y_P^*. The starting position of particle center locates on $(x_{p0}^* = 4, y_{p0}^* = 10)$ and the particle radius $r_p^* = 1$.

component of particle a_x^* keeps negative, and the particle will move to the left, and its velocity increases from zero; meanwhile, the liquid viscous force becomes larger. On the other hand, as the particle moves toward the central region of the optical ring, the repulsion force to particle from the left-side optical ring increases gradually, which counteracts a part of the dielectrophoresis force from the right-side optical ring and makes the total dielectrophoresis force smaller and smaller until the X-direction resultant force is reduced to zero, the combined acceleration also drops to zero, thus the particle velocity keeps relatively stable. When the particle reaches the center point of the optical ring, the repulsion forces from the two sides of optical rings achieve equilibrium; the X-component of dielectrophoresis force drops to almost zero. While the particle itself still owns a certain velocity, and it will be affected continuously by the liquid viscous force. Therefore, the total acceleration component a_x^* turns to a positive value, that is, its direction turns to the right, which will hinder particle translation toward left, make u_x^* decrease rapidly to zero, and finally, particle will park near the center point of the optical ring.

As shown in Fig. 10(b), when the starting position of the particle is far from the bottom edge, the dielectrophoresis force acting on particle is very feeble, and the liquid viscous force can be neglected considering the small particle velocity, so the combined acceleration of the particle is almost zero. As the particle continues to move downward, the dielectrophoresis force in the Y-direction increases rapidly, and the combined acceleration component a_y^* of the particles becomes greater, which leads to the downward velocity increasing quickly until its maximum value reaches. When the particle arrives at the bottom wall of micro-channel, the Y-component

Mod. Phys. Lett. B Downloaded from www.worldscientific.com
by CHALMERS UNIVERSITY OF TECHNOLOGY on 04/18/20. Re-use and distribution is strictly not permitted, except for Open Access articles.

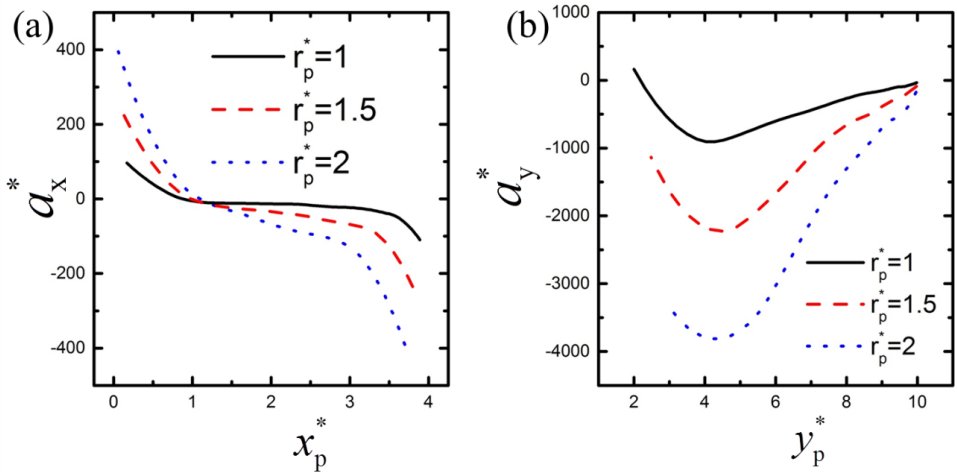

Fig. 10. (Color online) The particle acceleration with particle radius $r_p^* = 1, 1.5, 2$ depending on particle center position. (a) The X-component a_x^* of the particle acceleration depending on the particle center position x_P^*. (b) The Y-component a_y^* of the particle acceleration depending on the particle center position y_P^*. The starting position of the particle center locates on ($x_{p0}^* = 4$, $y_{p0}^* = 10$) and the applied AC voltage $\widetilde{\phi} = 30$ V.

of dielectrophoresis force turns to decreases rapidly as shown in Figs. 4 and 5. On the other hand, the interaction between the particle and the wall generates the additional wall-induced fluid resistance, both of them leads to the rapid decrease of a_y^* together, even it may change to a positive value, its direction turns to upward, particle begins to decelerate, which reduces the particle momentum and the impact effect in contact with the bottom wall.

In addition, as can be seen from Fig. 10, with the larger particle radius, the particle holds the greater acceleration during its whole motion process, which makes it easier to reach its maximum velocity, as shown in Figs. 8 and 9. Obviously, with the identical starting position and similar trajectory, the time spent by the particle with greater velocity will be less. In this way, particles with different radii can be separated easily.

4. Conclusion

When the polarization on a particle in an optically induced dielectrophoresis chip is weaker than that of solution, its motion is dominated by the negative dielectrophoretic force. The particle whose starting position is within the optical ring will move toward the center point of the ring. The dynamic process of particle in the horizontal direction is controlled by the dielectrophoretic force and the liquid viscous resistance. Besides, the dynamic process of particle in the vertical direction will be subjected to the additional disturbing effect of photoconductive layer on the electric field as well as the micro-channel wall on the flow field, especially when the

Mod. Phys. Lett. B Downloaded from www.worldscientific.com
by CHALMERS UNIVERSITY OF TECHNOLOGY on 04/18/20. Re-use and distribution is strictly not permitted, except for Open Access articles.

particle approaches the bottom edge of the micro-channel, significantly reducing the particle translation velocity and acceleration, which helps to reduce the impact effect of the particle in contact with the bottom wall.

The numerical results in this study illustrate the complete dynamic process of single circular particle in the ODEP chip in detail. The next step is to study the movement process and interaction mechanism of several or even a large number of biological particles in ODEP chip, which would further clarify the dynamic mechanism of biological particles for the massive and efficient manipulation by ODEP technology.

Nomenclature

$H = 100\ \mu$m,	height of microfluidic channel CDEF
$L = 200\ \mu$m,	length of microfluidic channel CDEF
$h = 2\ \mu$m,	thickness of the photoconductive layer ABFE
$\rho_f = 1000$ kg/m^3,	density of the deionized aqueous solution
$\varepsilon_f = 7.08 \times 10^{-10}$ F/m,	absolute permittivity of the deionized aqueous solution
$\sigma_f = 1 \times 10^{-3}$ S/m,	conductivity of the deionized aqueous solution
$\eta = 1 \times 10^{-3}$ Pa $\cdot$ s,	dynamic viscosity of the deionized aqueous solution
$\rho_p = 1050$ kg/m^3,	density of the polystyrene (PS) microsphere
$G_P = 1 \times 10^9$ Pa,	shear modulus of the polystyrene (PS) microsphere
$B_P = 1 \times 10^4$ Pa,	bulk modulus of the polystyrene (PS) microsphere
$\varepsilon_p = 2.3 \times 10^{-11}$ F/m,	absolute permittivity of the polystyrene (PS) microsphere
$\sigma_p = 4 \times 10^{-4}$ S/m,	conductivity of the polystyrene (PS) microsphere
$r_P = 5, 7.5, 10\ \mu$m,	particle radius
$d_r = 40\ \mu$m,	inner diameter of the ring-shaped light source
$d_R = 50\ \mu$m,	outer diameter of the ring-shaped light source
$\varepsilon = 11.7\varepsilon_0$,	absolute permittivity of α-Si:H (F/m)
ε_0,	absolute permittivity in vacuum (F/m)
$\sigma_l = 0.21$ S/m,	conductivity in the bright region of the photoconductive layer
$\sigma_d = 6.7 \times 10^{-5}$ S/m,	conductivity in the dark region of the photoconductive layer
$f = 10^5$ Hz,	alternative frequency of the AC voltage
$\tilde{\varepsilon}_f = \varepsilon_f - j\sigma_f/\omega$, $\tilde{\varepsilon}_p = \varepsilon_p - j\sigma_p/\omega$, $\tilde{\varepsilon}_l = \varepsilon - j\sigma_l/\omega$, $\tilde{\varepsilon}_d = \varepsilon - j\sigma_d/\omega$,	the complex permittivity of fluid, particle, bright area and dark area, respectively (F/m)
$\omega = 2\pi f$,	angular frequency of AC(Hz)
$j = \sqrt{-1}$,	imaginary part unit
$\widetilde{\phi}_f, \widetilde{\phi}_p, \widetilde{\phi}_l, \widetilde{\phi}_d$,	the complex potential in fluid, particle, bright area and dark area, respectively (V)
$\mathbf{n}$,	unit normal vector
$\mathbf{u}$,	fluid velocity (m/s)
a,	acceleration velocity (m/s^2)

Mod. Phys. Lett. B Downloaded from www.worldscientific.com
by CHALMERS UNIVERSITY OF TECHNOLOGY on 04/18/20. Re-use and distribution is strictly not permitted, except for Open Access articles.

p,	fluid pressure (Pa)
t,	time variable (s)
$\mathbf{T}_M$,	Maxwell stress tensor (N/m)
$\mathbf{T}_H$,	hydrodynamic stress tensor (N/m)
$\mathbf{F}_{\mathrm{DEP}}$,	time-averaged dielectrophoresis force (N)
$\mathbf{F}_H$,	liquid viscous resistance (N)
$\widetilde{\mathbf{E}}$,	intensity of the electric field (V/m)
$\widetilde{\mathbf{E}}'$,	complex conjugate of $\widetilde{\mathbf{E}}$ (V/m)
m_p,	particle mass (kg)
x_p,	x-coordinate position of particle center (μm)
x_{p0},	starting position of particle center (μm)
$\mathbf{U}_p$,	translation velocity of particle(m/s)
R_0,	universal gas constant, J/(mol $\cdot$ K)
T,	absolute temperature (K)
F,	Faraday constant (C/mol)
Re,	Reynolds number
$\widetilde{f}_{\mathrm{CM}}$,	complex Clausius–Mossotti factor
$\lvert\widetilde{\mathbf{E}}_{\mathrm{rms}}\rvert$,	root mean square of the electric field (V/m)

Subscripts:

f,	fluid filled in the microfluidic channel
P,	PS particle
r,	inner diameter of the ring-shaped light source
R,	outer diameter of the ring-shaped light source
l,	bright region of the photoconductive layer
d,	dark region of the photoconductive layer
M,	Maxwell
H,	hydrodynamic
DEP,	dielectrophoresis

Superscripts:

$\sim$,	complex variable
$*$,	dimensionless variable
$\prime$,	conjugate

Acknowledgments

This work is funded by Hainan Provincial Natural Science Foundation of China (Grant Nos. 519MS021 and 2019RC032), National Natural Science Foundation of China (Grant Nos. 61964006 and 51605124) and National Research Foundation of Korea (NRF-2018R1A2B3001246).

Mod. Phys. Lett. B Downloaded from www.worldscientific.com
by CHALMERS UNIVERSITY OF TECHNOLOGY on 04/18/20. Re-use and distribution is strictly not permitted, except for Open Access articles.

References

1. K. K. Hyoung, X. Xuan and Y. Kang, *J. Appl. Phys.* **99** (2006) 064702.
2. Y. X. Song, J. D. Yang and X. F. Shi, *Sci. China Chem.* **55** (2012) 524.
3. P. Garcìa-Sánchez, Y. Ren and J. J. Arcenegui, *Langmuir* **28** (2012) 13861.
4. Y. Ai, A. Beskok and D. T. Gauthier, *Biomicrofluidics* **3** (2009) 044110.
5. J. Zhu and X. Xuan, *Electrophoresis* **30** (2009) 2668.
6. H. Zhou, L. R. White and R. D. Tilton, *J. Colloid Interf. Sci.* **285** (2005) 179.
7. D. Das, K. Biswas and S. Das, *Med. Eng. Phys.* **36** (2014) 726.
8. R. Pethig, *Crit. Rev. Biotech.* **16** (1996) 331.
9. Y. Ai, Z. Zeng and S. Qian, *J. Colloid Interf. Sci.* **417** (2014) 72.
10. J. Lu, H. Yang and L. Zhou, *Phys. Rev. Lett.* **118** (2017) 043601.
11. M. G. Moisescu, T. Savopol and L. Dimitriu, *Anal. Chim. Acta* **1030** (2018) 166.
12. T. Zhou, Y. Deng and H. Zhao, *J. Fluids Eng.* **140** (2018) 091302.
13. T. Zhou, L. Shi and C. Fan, *Microfluid. Nanofluid.* **21** (2017) 59.
14. T. Zhou, X. Ji and L. Shi, *Electrophoresis* **40** (2019) 993.
15. P. Y. Chiou, A. T. Ohta and M. C. Wu, *Nature* **436** (2005) 370.
16. A. T. Ohta, P. Y. Chiou and T. H. Han, *J. Microelect. Syst.* **16** (2007) 491.
17. A. T. Ohta, P. Y. Chiou and H. L. Phan, *IEEE J. Sel. Top. Quantum Electron.* **13** (2007) 235.
18. P. Y. Chiou, A. T. Ohta and A. Jamshidi, *J. Microelect. Syst.* **17** (2008) 525.
19. W. Y. Lin, Y. H. Lin and G. B. Lee, *Microfluid. Nanofluid.* **8** (2010) 217.
20. H. Hwang, D. H. Lee and W. Choi, *Biomicrofluidics* **3** (2009) 014103.
21. H. Hwang and J. K. Park, *Lab on a Chip* **9** (2009) 199.
22. X. L. Zhu, Z. F. Yin and Z. Q. Gao, *Sci. China Technol. Sci.* **53** (2010) 2388.
23. S. Hu, Y. Zhao and Q. Wang, *Optik* **126** (2015) 3240.
24. S. H. Hung, S. C. Huang and G. B. Lee, *Sensors* **13** (2013) 1965.
25. W. Liang, N. Liu and Z. Dong, *Sensors Actuat. A: Phys.* **193** (2013) 103.
26. Y. Zhao, S. Hu and Q. Wang, *Microfluid. Nanofluid.* **17** (2014) 287.
27. T. Zhou, X. Ji and L. Shi, *Electrophoresis* (2019), https://doi.org/10.1002/elps.201900266.
28. T. Zhou, J. Ge and L. Shi, *Electrophoresis* **39** (2018) 590.
29. H. W. Wu, Y. S. Huang and H. Y. Lee, *Biomed. Microdevices* **18** (2016) 79.
30. J. F. Muñoz-Martínez, J. B. Ramiro and Á. Alcázar, *Phys. Rev. Appl.* **7** (2017) 064027.
31. W. P. Chou, H. M. Wang and J. H. Chang, *Sensors Actuat. B: Chem.* **241** (2017) 245.
32. T. K. Chiu, A. C. Chao and W. P. Chou, *Sensors Actuat. B: Chem.* **258** (2018) 1161.
33. P. Y. Chu, C. J. Liao and C. H. Hsieh, *Sensors Actuat. B: Chem.* **283** (2019) 621.
34. X. Zhu, Z. Yin and Z. Ni, *Microfluid. Nanofluid.* **12** (2012) 529.
35. J. P. Hsu, L. H. Yeh and Z. S. Chen, *J. Colloid Interf. Sci.* **310** (2007) 281.
36. J. P. Hsu, L. H. Yeh and M. H. Ku, *J. Colloid Interf. Sci.* **305** (2007) 324.
37. J. P. Hsu, Z. S. Chen, M. H. Ku and L. H. Yeh, *J. Colloid Interf. Sci.* **314** (2007) 256.
38. Y. Zhao, S. Hu and Q. Wang, *Microfluid. Nanofluid.* **16** (2014) 533.
39. S. L. Neale, M. Mazilu and J. I. B. Wilson, *Opt. Exp.* **15** (2007) 12619.